JOURNAL OF GEOPHYSICAL RESEARCH, VOL. 106, NO. C5, PAGES 9213–9222, MAY 15, 2001

"Upwelling" and "cyclonic" regimes of the near-surface circulation in the Santa Barbara Channel

Lie-Yauw Oey,[1] Dong-Ping Wang,[2] Thomas Hayward,[3] Clinton Winant,[4] and Myrl Hendershott[4]

Abstract. The observed near-surface circulation in the Santa Barbara Channel indicates in particular two patterns: a dominant cyclonic circulation mode and a less frequent upwelling flow mode. To explain the dynamics that may govern these two flow regimes, momentum balance from a hindcast model of currents in the channel, forced by observed hourly winds and hydrographic data, was calculated. The along-channel balance was found to be between wind, which was eastward (i.e., equatorward), sea level tilt, which was westward (i.e., poleward), and Coriolis, which was westward if the wind was (1) intense west and east of the channel and was eastward if the wind was (2) weaker in the east. Wind condition 1 produced southward cross-channel flow in the midchannel, connected by eastward currents upstream (downstream) along the northern (southern) coast of the channel, while wind condition 2 produced northward cross-channel flow connected by cyclonic recirculation in the west and westward inflow in the east. It is suggested that the former corresponds to the dynamical balance that may occur in the upwelling flow mode, while the latter corresponds to the cyclonic circulation mode.

1. Introduction

The Santa Barbara Channel (SBC; Figure 1) is located at the confluent region between the warm water of Southern California Bight (SCB) origin and cooler upwelled water off the central California coast. The channel's orientation is approximately west to east so that westward (eastward) along the channel is synonymous to poleward (equatorward), and we will freely interchange their usage when referring to circulation in the channel. The region is partially sheltered from the often intense (especially in summer) north and northwesterly wind by the mountain range along the channel's northern coast, so there can be large differences in wind strengths from west (stronger) to east along the channel [*Winant and Dorman*, 1997]. Thus the channel's circulation can be expected, at least near the surface (defined to be from approximately 5 to 45 m below the surface as delineated by observed current meter depths), to depend on a combination of wind, wind curl, and thermal contrast. While equatorward winds generally drive coastal currents near the surface equatorward [*Allen*, 1980], the situation in the SBC/SCB is complicated by the observed fact that the wind curl near Point Conception is very intense, often in excess of 0.1 N m^{-2} per 100 km (C. E. Dorman, private communication, 1998), and that this diminishes equatorward along the channel and farther south along the SCB coast. The equatorward weakening of the wind curl, which on the seasonal timescale peaks in summer, generates a poleward pressure gradient that drives poleward coastal flow [*Oey*, 1996, 1999]. Thus nearshore flows in the SCB, including flows through SCB, can be thought of as being driven by these two competing (and inseparable) mechanisms. The theory was originally intended to apply to seasonal timescales (and large spatial), but a more careful scaling analysis by *Oey* [1999] suggests that it should also be applicable to shorter timescales (O(10 days)) and spatial (channel) scales.

Though the above idea can explain the origin of the alongshore pressure gradients (please see *Hickey* [1992], *Auad and Hendershott* [1997], and *Oey* [1999] for other possible origins of the alongshore pressure gradient, for example, remote forcing and sea level setup), it does not address how the imbalances of these and the wind drive the channel's circulation. *Harms and Winant*'s [1998] analysis of the 1994/1995 observations shows that near-surface currents in the channel are indeed a function of both wind and along-channel pressure gradient. They noted that flow in the channel had a strong tendency of being cyclonic, westward (eastward) along the northern (southern) coast especially in the western portion of the channel. This cyclonic circulation mode exists through a wide range of values of wind and along-channel pressure gradient forcing combinations. There are exceptions, however; under certain wind and pressure gradient combinations in which the cyclonic mode is replaced (or weakened) by more or less unidirectional flows through the channel, either poleward or equatorward. These conditions prevail in spring when wind is equatorward both in the west and in the eastern portion of the channel, as well as farther south in the SCB, and in winter with passages of storms. *Harms and Winant* [1998] further classified what we loosely term here as "unidirectional flow" scenarios into three categories: (1) upwelling, when currents are equatorward at either end of the channel and along its southern coast and weakly poleward along the northern coast, (2) relaxation, when a strong poleward jet extends from the channel's eastern end and northwestward across the channel to the northern coast while

[1]Atmospheric and Oceanic Science Program, Princeton University, Princeton, New Jersey.
[2]Marine Science Research Center, State University of New York at Stony Brook, Stony Brook, New York.
[3]Marine Life Research Group, Scripps Institute of Oceanography, La Jolla, California.
[4]Center for Coastal Studies, Scripps Institute of Oceanography, La Jolla, California.

Paper number 1999JC000129.
0148-0227/01/1999JC000129$09.00

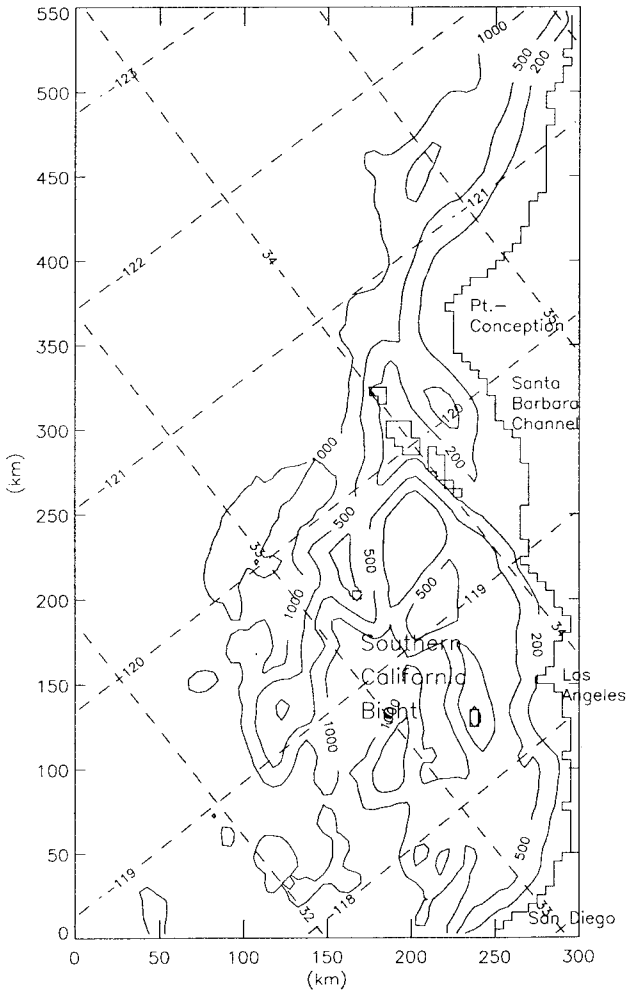

Figure 1. SBC and SCB locator map and the model domain and topography. For computational efficiency the deepest model's depth has been set to 2000 m.

the flow along the southwestern shelf is weakly equatorward, and (3) floods, when currents are either equatorward or poleward on both sides of the channel. The upwelling and relaxation (as well as cyclonic) regimes occur predominantly from spring through fall, while floods are most often associated with passages of transient winter storms. While these different classifications seemed reasonable, the consensus now amongst us (led by Winant) is that they may be redundant, especially in light of the current patterns revealed by considerations of wind and pressure gradient forcing [see *Harms and Winant*, 1998, Figure 16], which suggest that they may all share a common dynamical theme. Nevertheless, the results described herein approximate only the upwelling and cyclonic flow scenarios, henceforth referred to as regimes I and II, respectively. Our objective is to conduct model experiments to understand the dynamics of these two flow regimes.

Our analyses will be to compute momentum balance on the basis of an application of the *Oey*'s [1996] SBC/SCB model forced by observed hourly wind stresses and California Cooperative Oceanic Fisheries Investigations (CalCOFI) temperature T and salinity S fields, from December 1997 through April 1998, a period of intense hydrographic surveys. The choice of a model with realistic bathymetry and forcing, as opposed to a model with idealized settings, offers the advantage that inferences that are specific to the SBC/SCB system can be made. The downside is that the analysis will be more complex, and simplifications will be made. The present note will focus on understanding the dynamics of the two observed flow regimes described above. Detailed model/data comparison will be described in a separate paper. Section 2 describes the model, boundary conditions, and forcing; section 3 describes results and balance analyses; and section 4 provides conclusion.

2. Methodology

To infer circulation dynamics, we use data, buoy winds, and CalCOFI hydrographic surveys to force an ocean model that solves the three-dimensional structure and temporal evolution of currents, temperature, and salinity, assuming that the ocean is incompressible and hydrostatic and using the Boussinesq approximation [*Oey and Chen*, 1992]. The model boundary conditions, domain, and topography are the same as those used by *Oey* [1996, Figure 1], with two exceptions. The present application employs the coarse-grid only (i.e., the nested grid option is turned off), with grid sizes $\Delta x = \Delta y = 5$ km and 30 equally spaced sigma layers in the vertical. Second, a 200 km wide sponge layer, within which the horizontal viscosity is linearly increased to 10 times its interior value, is placed along the western open boundary. In combination with a radiation condition the sponge damps westward propagating Rossby waves and helps to prevent the development of an artificial boundary current.

2.1. Initial Condition and *T*/*S* Assimilation

Integration began on December 16, 1997, and ended on May 5, 1998. The initial T and S fields were obtained from the monthly climatological data set for December. The monthly T/S fields were also used as boundary conditions during the integration. However, to account for the actual T/S conditions in 1997/1998, CalCOFI data from December 1997 and February–March 1998 cruises were assimilated into the model. While there were a number of cruise tracks, line 90 (which spans offshore from the coast between Los Angeles and San Diego; Plate 1) only was used. The rationale is that T/S forcing from this southern location would propagate north to influence circulation in the channel. If CalCOFI T/S in and/or near the channel are also assimilated, questions related to incompatibility of data in the channel must also be addressed as the model attempts to adjust both to local and to remote forcing, and dynamical interpretations will be more difficult.

The assimilation was accomplished as follows [cf. *Chen and Wang*, 1999]. The CalCOFI data at each standard level were first interpolated onto the model grid using

$$T_{ci} = \sum T_{cn} E_{ni} \Big/ \sum E_{ni} \tag{1a}$$

$$E_{ni} = \exp\{-[(x_{cn} - x_i)/x_s]^2 - [(y_{cn} - y_i)/y_s]^2\}, \tag{1b}$$

where the summation Σ is over the total number N of CalCOFI data points (i.e., $n = 1, N$), T_{ci} denotes the interpolated value at the model's ith grid point (x_i, y_i) (in degrees longitude and latitude, say), T_{cn} denotes the nth station CalCOFI value at (x_{cn}, y_{cn}), and x_s and y_s are parameters that dictate the radius of influence of the CalCOFI data on the neighboring model grid points. Here we take $x_s = y_s = 0.25°$.

Assimilated fields T_{ai} are next constructed using a weighted

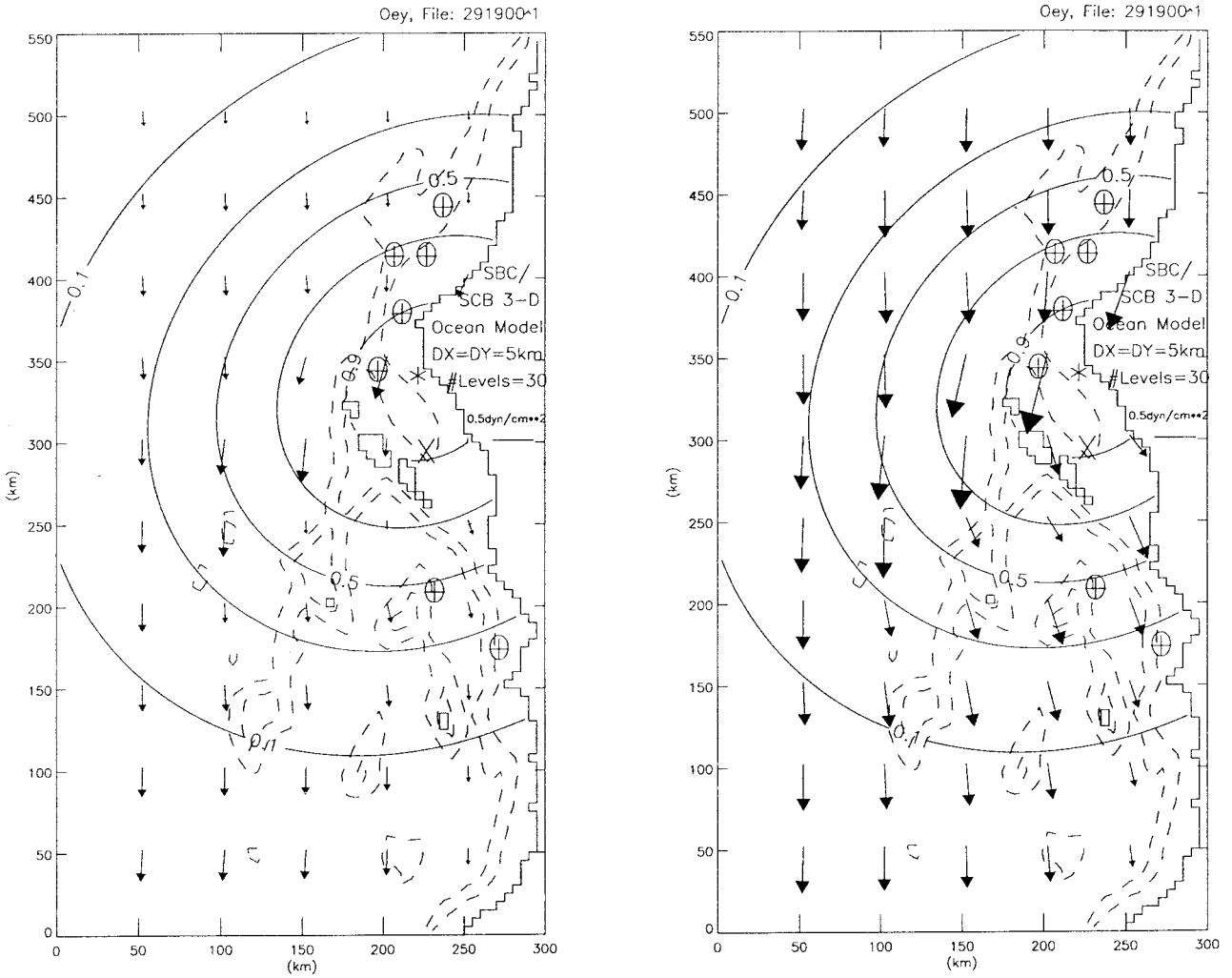

Figure 2. The 10 day averaged wind vectors on January 15 and April 15, 1998. Locations of NDBC wind stations used in the simulation are marked as a circled plus. They are, from northwest to southeast, 46062, 46011, 46023 (offshore), PTGC1, 46054, 46025 (offshore), and 46045. An additional station, marked as a cross (NDBC station 46053) was also used (see text). The location of center of gravity of these stations is marked with an asterisk. The contours give the weighting function used to merge the NDBC with COADS winds (see text).

combination of the interpolated CalCOFI values T_{ci}, and historical values T_{hi}:

$$T_{ai} = W_i T_{ci} + (1 - W_i) T_{hi}, \tag{2a}$$

$$W_i = \exp[-\min_n (R_{ni})] \cdot \exp[(Z_i/200) - H_v(t - t_o)(t - t_o)/30], \tag{2b}$$

$$R_{ni} = [(x_{cn} - x_i)/x_s]^2 + [(y_{cn} - y_i)/y_s]^2, \tag{2c}$$

where the minimum function, min, checks over the total number N of CalCOFI data points, z_i is the vertical coordinate (=0 at surface and $=-H(x, y)$, where H is water depth, at the ocean bottom) in meters, t is time in days, t_o is time that corresponds to April 15, 1998, and H_v is the Heaviside function. The spatial distribution of the weighting function W_i is such that near the surface it is ≈1 for model grid points near any of the CalCOFI stations but decays exponentially away and also with depth (as well as linearly with time after April 15). Thus the assimilated field T_{ai} assumes CalCOFI for grid points near the cruise stations in the upper 200 m (for depths below 200 m the T/S approximately equal historical T_h/S_h) and merges smoothly to historical field for position far away. Finally, the assimilated field is inserted into the T/S transport equations as "sources" (i.e., the model was used in a so-called "robust diagnostic mode"):

$$\partial T/\partial t = \cdots + C(T_a - T) \tag{3a}$$

$$C = W_i|_{z=0}[G_d + (G_s - G_d) \exp(z/500)], \tag{3b}$$

where $G_s = 1/5\ \mathrm{d}^{-1}$ and $G_d = 1/300\ \mathrm{d}^{-1}$ and similarly for S. Thus for grid points near CalCOFI the modeled T/S are nudged back to CalCOFI ($W_i|_{z=0} \approx 1$) with timescales of 5 days near the surface and 300 days in deeper layers [cf. *Oey and Chen*, 1992]. Away from CalCOFI stations the T/S are nudged toward the historical T/S (because of (2)) but at increasing timescales ($W_i|_{z=0} < 1$); the calculation becomes essentially prognostic for distances >50 to 100 km away, in SBC in particular. In Plate 1 we compare the near-surface temperature fields on January 5, 1998, for runs with and without the CalCOFI nudging. It shows that because of 1997 El Niño influence, the temperature with CalCOFI nudging is 1°–2°C higher than "climatology" especially near the coast. By this time (20

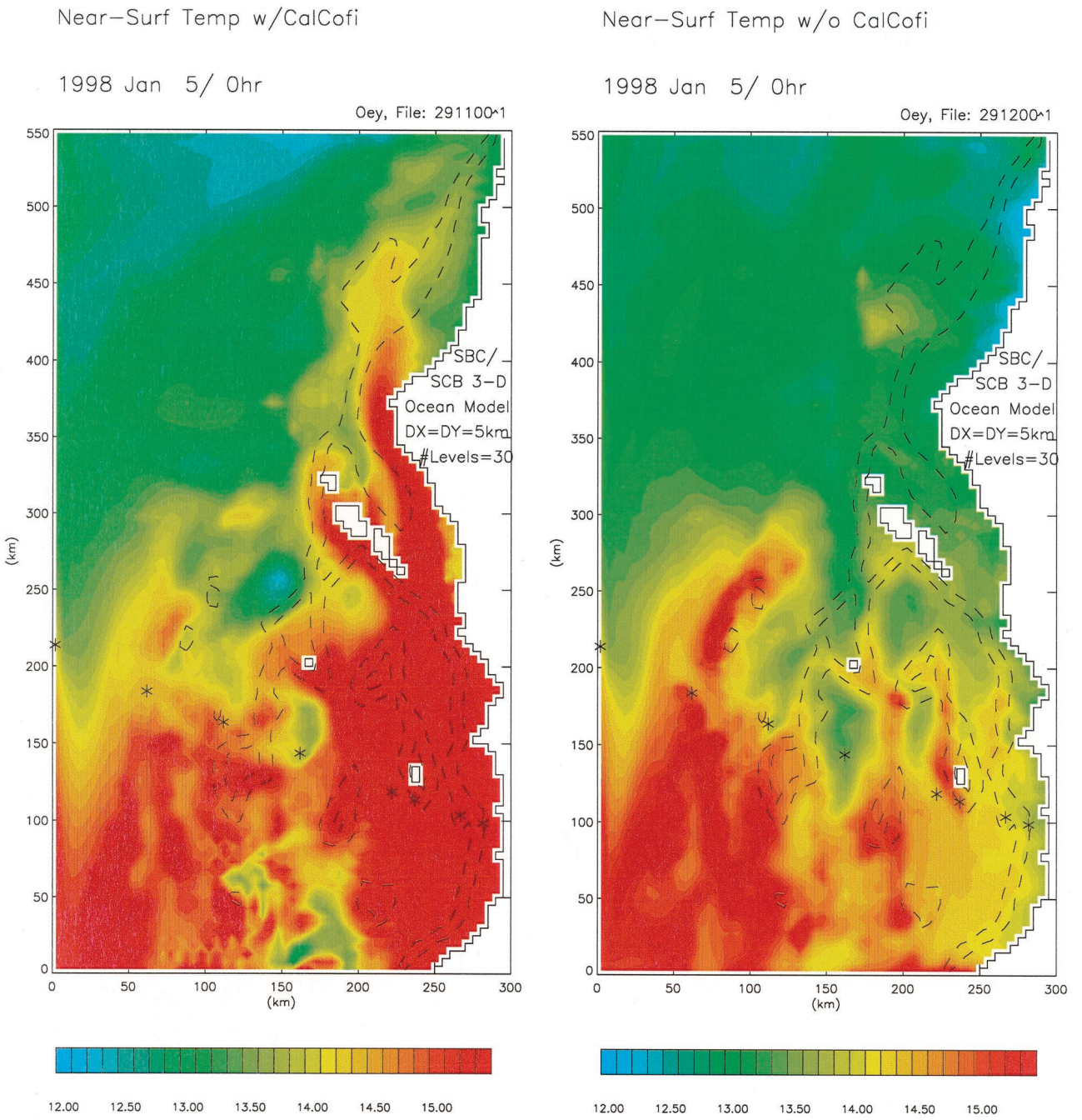

Plate 1. A comparison of the temperature fields at the first near-surface sigma level on January 5, 1998, (left) with and (right) without assimilation of the CalCOFI T/S along line 90 (the starred points).

days into the integration) the warmer water has intruded into the channel and past Point Conception.

2.2. Wind

The wind was specified by merging the observed hourly wind vectors $\mathbf{U_w}$ at National Data Buoy Center (NDBC) stations in the vicinity of the channel (see Figure 2 for station sites) with climatological winds from Comprehensive Ocean-Atmosphere Data Sets (COADS) that cover the entire model domain (and beyond) as follows. The NDBC winds were first converted to wind stresses using *Large and Pond*'s [1981] formula:

$$\tau_o = C_d|U_w|U_w \qquad \mathrm{m^2\ s^{-2}}, \tag{4}$$

where $C_d = 1.44 \times 10^{-6}$ for $|\mathbf{U_w}| < 11$ m s^{-1} and $|\mathbf{U_w}| = (0.49 + 0.065\,|\mathbf{U_w}|) \times 10^{-6}$ otherwise. These were interpolated onto the model grid points using (1) with $x_s = y_s = 1.5°$ and merged with COADS wind using (2a) (i.e., with NDBC replacing T_{ci} and COADS replacing T_{hi}). However, the weighting function is simpler, $=E_{ni}$, where the (x_{cn}, y_{cn}) in (1b) is taken as fixed equal to (−120°12′, 34°24′), the center of gravity of the NDBC sites used.

2.3. Two Different Wind Experiments

For the simulation period, NDBC winds were available at seven sites in the vicinity of the channel (those marked a circled plus in Figure 2) but was missing at station 46053

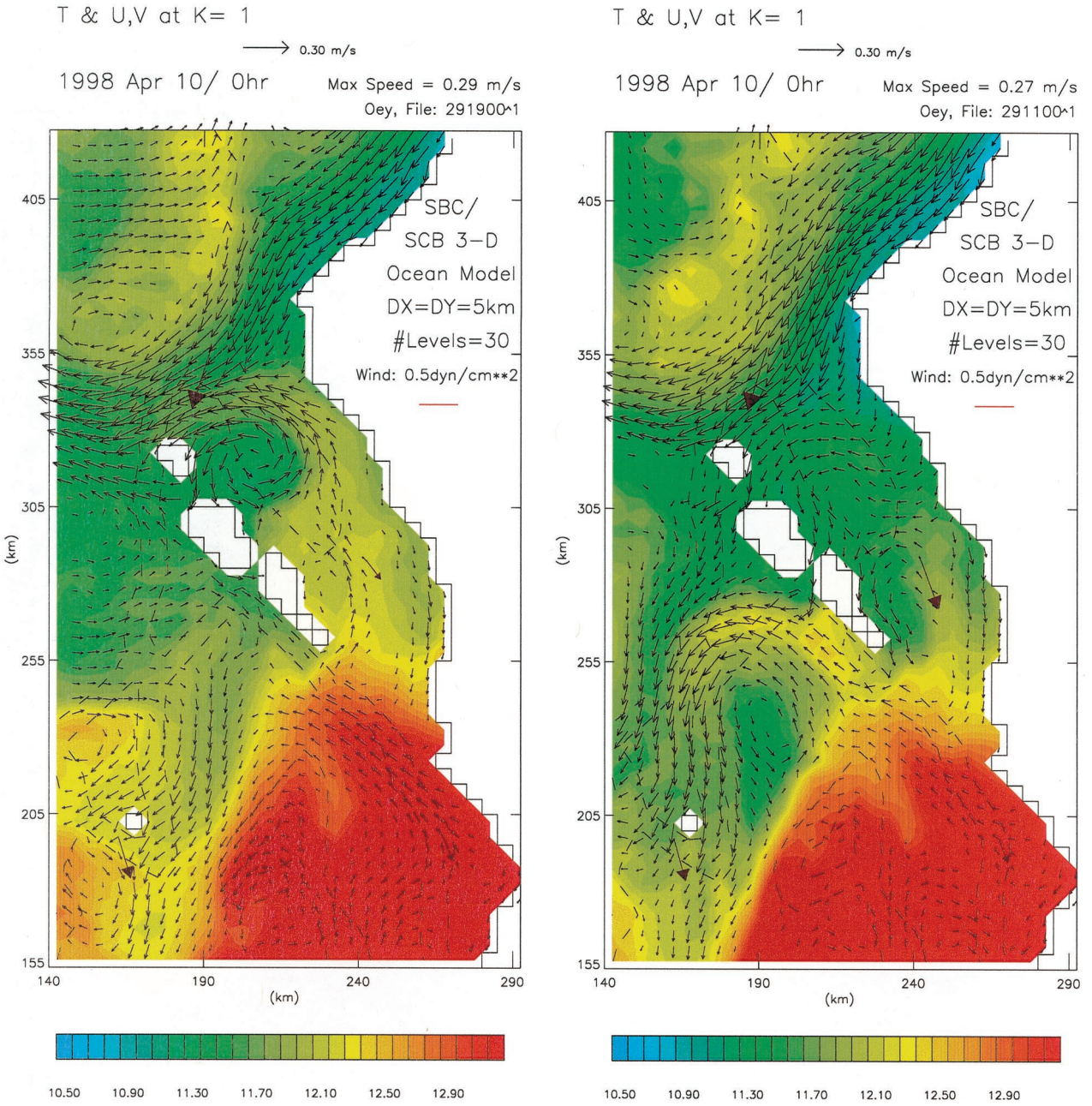

Plate 2. The 10 day averaged temperature (°C) and currents at the first model grid point near the surface, and centered on April 10, 1998 for (left) experiment A and (right) experiment B, in an enlarged region that focuses on the Santa Barbara Channel and vicinity. Averaged wind stresses are also plotted as vectors with thick arrows at four locations (see text).

(marked by a cross). Wind observations in other years [*Dorman and Winant*, 2000] indicate that the wind at this missing station is generally weak, more like winds farther south and southeast. This happens, in general, during late spring/early summer to fall. During early spring the wind at station 46053 is generally intense like winds in the western channel. Theory [*Oey*, 1999] suggests that detailed wind distribution inside the channel would be important to the local circulation, and it is of interest to test the above two different wind scenarios at station 46053. In one experiment (A in Table 1), wind at station 46053 was equated to that farther south at station 46045. This resulted in winds in the east weaker than winds in the west of the channel. Figure 2 shows an example of the wind for this experiment at two times, winter and spring. The wind in spring is more intense (than in winter); both, however, show similar wind weakening from west to east of the channel and also to the south over the SCB. In another experiment (B in Table 1), wind at 46053 was not explicitly set but was interpolated as described previously. Because of the proximity of station 46053 to the western channel station 46054, the interpolation gives a more uniform wind in the channel (not shown) in that wind east of the channel becomes more similar to that in the west, and wind throughout the channel becomes generally more intense (and equatorward) than that used for experiment A.

Table 1. Model Experiments[a]

Experiment	Winds		T/S Assimilation		Wind Merging Scales X_s and Y_s	NDBC Buoy 46053 Setting
	COADS	NDBC	Historical	CalCOFI		
A	*	*	*	*	1.5°	46045
B	*	*	*	*	1.5°	—
C	*	*	*	—	1.5°	46045
D	*	*	*	—	1.5°	—
E	*	*	*	*	3.0°	46045
F	*	*	*	*	1.5°	46025

[a]An asterisk or number means that the item was applied in the model. A dash means that the item was omitted.

The upshot is that experiment A has a larger differential wind curl (more cyclonic west than east) along the channel, hence a tendency for a stronger poleward pressure gradient, than experiment B. Therefore, as mentioned previously, experiment B typifies an early spring wind scenario, and experiment A typifies a situation that occurs most often during late spring through summer and fall.

3. Results

Observations [*Hayward et al*., 1999] (and model results; see below) indicate a distinct change in hydrography from the El Niño–dominated period, December 1997 to February 1998, when poleward near-coast flow brought warm water past Point Conception (e.g., Plate 1), to a more typical spring period, March–April 1998, during which strong equatorward wind prevails and upwelling jet appears along the central California coast (north of Point Conception). We will focus on this spring period and, as discussed previously, also on the near-surface currents. Plate 2 compares currents and temperatures at the first sigma grid point near the surface, 10 day averaged around April 10, 1998, for experiment A (Plate 1 (left)) and experiment B (Plate 1 (right)). For clarity an enlarged domain focusing only on the SBC is shown in Plate 2, as opposed to the full domain shown in previous figures (see Figure 1). Averaged wind stresses are also superimposed as full arrow vectors at four locations: west and east of the channel and offshore and near-shore along $y \sim 195$ km in the SCB. Note that the wind diminishes more drastically from west to east along the channel for experiment A than for experiment B. Plate 2 shows cool waters (≈10°–13°C from north to south) along the coast and inside SBC. In contrast, in January, when warmer waters related to effects of El Niño prevailed, temperatures in the vicinity of the channel were 2°–5°C higher (see Plate 1; note the different temperature scales; see Figure 1 for location of the channel), with largest differences occurring in the SBC and along the central California coast. Plate 2 also shows that currents off the central California coast are equatorward in both experiments. The main difference between the two experiments is inside the channel. For experiment A (Plate 2 (left)) a poleward current or "jet" extends from the eastern entrance just off the island chain to the northwest shelf with the appearance of a distinct cyclone in the west. There are also equatorward currents over the shallow (water depths <100 m) shelf in the northeastern part of the channel because of local upwelling forced by near-coast equatorward wind. This local upwelling also exists for experiment B (Plate 2 (right)) and, in fact, is a little more intense, as can be expected because of the stronger wind specified over the eastern portion of the channel in that experiment. Apart from this localized upwelling region, the circulation patterns in the two experiments are quite different in the main channel proper. Foremost is the disappearance of the western cyclone in experiment B and the absence of the poleward current extending from east to the northwest shelf. Instead, the cross-channel flow is predominantly southward, and along-channel currents are equatorward all along the southern coast and, though much weaker, also off the northwest shelf. The absence of the poleward current in experiment B results in less warm water being transported through the channel ($T \approx 11$°C for experiment B compared to $T \approx 12$°C for experiment A near midchannel). This reversal of the net along-channel flow, from poleward for experiment A to equatorward for experiment B, is summarized in Figure 3, which compares the width-averaged (see also below) along-channel velocities as a function of distance along the channel. For experiment A, flow is predominantly poleward, more intense toward the western end of the channel because of the poleward jet and the (asymmetric) cyclone described above in connection with Plate 2. In contrast, flow is dominantly equatorward for experiment B. The contrast signifies a basic change in the model dynamics that we will discuss next. We should also mention that the circulation patterns shown in Plate 2 and the net flow shown in Figure 3 are robust in the sense that clear distinctions exist between the two experiments regardless of the averaging periods (from 1 to 30 days), provided that they include March and/or April, when the winds are intensely equatorward, and also that the averaging is calculated some 60 days after the initial transients.

3.1. Momentum Balance

We resolved the model velocities in the near-coast region into cross-isobath (x and u; positive shoreward, i.e., northward across the channel) and along-isobath (y and v; positive poleward, i.e., westward along the channel) components. We find that the cross-isobath momentum balance is to a good approximation geostrophic. The along-isobath momentum equation is

$$\underset{\text{I}}{dv/dt} + \underset{\text{II}}{fu} + \underset{\text{III}}{g \cdot \partial\eta/\partial y} - \underset{\text{IV}}{\partial(K \cdot \partial v/\partial z)/\partial z} + \underset{\text{V}}{(g/\rho_o) \cdot \int_z^0 \partial\rho/\partial y \cdot \partial z'} = 0, \quad (5)$$

where $d/dt = \partial/\partial t + \mathbf{u} \cdot \nabla$, K is the eddy viscosity coefficient ($m^2\ s^{-1}$), ρ is the density (kg m^{-3}), $g = 9.8$ m s^{-2}, f is the Coriolis parameter (s^{-1}), and a small term arising from the curvature of the isobath (coastline) is omitted. Each term in (5)

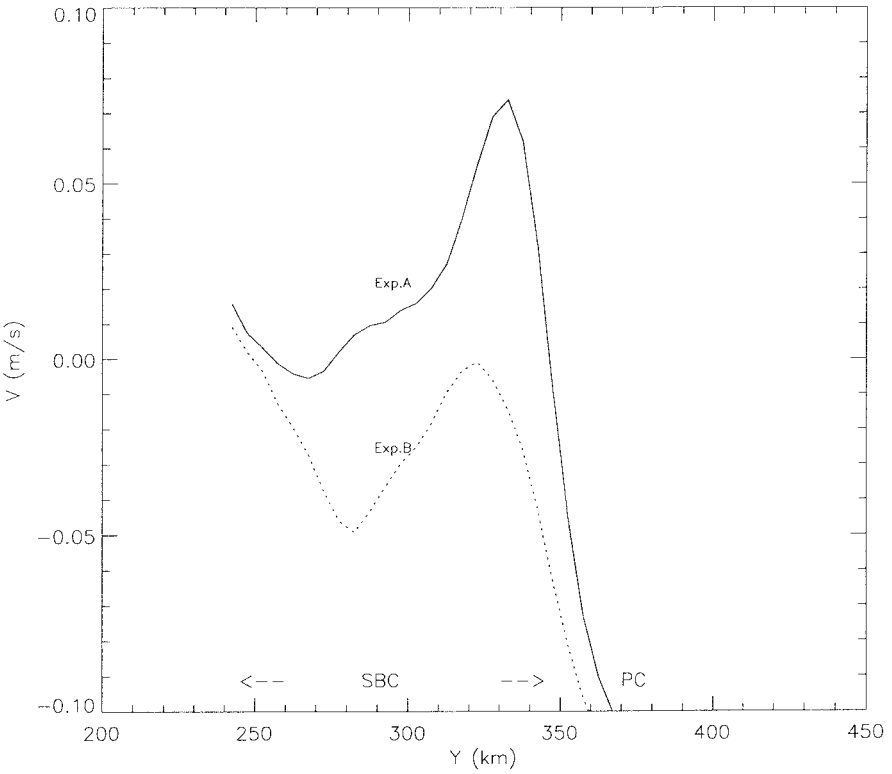

Figure 3. A comparison of the width-averaged along-channel velocities near the surface corresponding to the circulation patterns shown in Plate 2, as a function of distance along the channel, for experiment A (solid) and experiment B (dotted). Geographical locations along Y are SBC and Point Conception (PC).

was calculated beginning with the 50 m isobath near the coast, and to 40 km offshore, and averaged cross shore (note that in the SBC this averaging encompasses the entire channel width). In this paper we focus on quasi-steady balance for which term I is small. We found that the magnitude of term I was smaller than 5% of the sea level slope (term III) when (5) was averaged over 10 days or more. As in Plate 2, the result is insensitive to this averaging period, provided that it included March and/or April. Moreover, term V was found to be also small for the near-surface layers (<50 m) for which we wish to explain the different flow regimes arising from experiment A and experiment B. The three remaining terms represent (1) the force per unit mass, positive equatorward, due to Coriolis (term II), (2) the pressure gradient or sea level slope (term III), and (3) the predominantly wind-induced vertical shear (term IV, negative sign included). These are plotted for the near-surface grid in Figures 4a (experiment A) and 4b (experiment B) as a function of the alongshore distance. Plotted is also the term that represents friction acting at the base of the near-surface layer; i.e., the term IVb on the right-hand side of

$$-\partial(K\cdot\partial v/\partial z)/\partial z \approx -\tau_o^y/\Delta z + (K\cdot\partial v/\partial z)\big|_{\text{base}}/\Delta z, \qquad (6)$$

$$\text{IV} \qquad \text{IVa} \qquad \text{IVb}$$

where τ_o^y is the along-isobath wind stress and Δz ($\approx$15 m) is the thickness of the layer. Figure 4 shows that this friction term is small in comparison to the total shear term IV. Wind stress therefore dominates term IV and is equatorward along the entire coast (i.e., term IVa is positive). Thus, to a good approximation the alongshore balance is between the wind (IVa $\approx$ IV; dashed curves), pressure gradient (III; dotted curves), and Coriolis (II; dash-dotted curves) terms. We note also that the friction term IVb is negative (dash–triple-dotted curves), which means that the alongshore currents near the surface, being wind-driven, are more equatorward than currents in the lower layer. This is true for both experiments (and also for all other sensitivity experiments listed in Table 1), and the frictional force is poleward, opposing the wind.

The momentum balance calculations (Figure 4) can now be used to understand the differences in the flow field shown in Plate 2 and Figure 3 between experiments A and B. Over the eastern third of the channel ($y \approx 250$–280 km in Figure 4), wind stress in experiment A and hence its offshore Ekman flux (i.e., southward across the channel, or $u < 0$) remains weak and approximately equal to its values farther east and south in the SCB (not shown; recall that for experiment A, wind at eastern station 46053 was equated to that at station 46045 in the SCB). The equatorward wind intensifies farther west and reaches a maximum in the western mouth of the channel near Point Conception (PC; Figure 4a). This poleward intensification of wind also exists in experiment B (Figure 4b) with important differences that (1) the increase is more gradual and (2) the magnitude is 2–3 times stronger throughout the channel. The reason is, as described previously, wind in the channel for experiment B is more uniformly distributed through the channel, and there exists a more gradual transit to weaker winds in the SCB. The equatorward winds in both experiments would induce, when other forcing is small, equatorward coastal currents along the north and south coasts of the channel, connected by a southward cross-channel flow ($u < 0$). This is

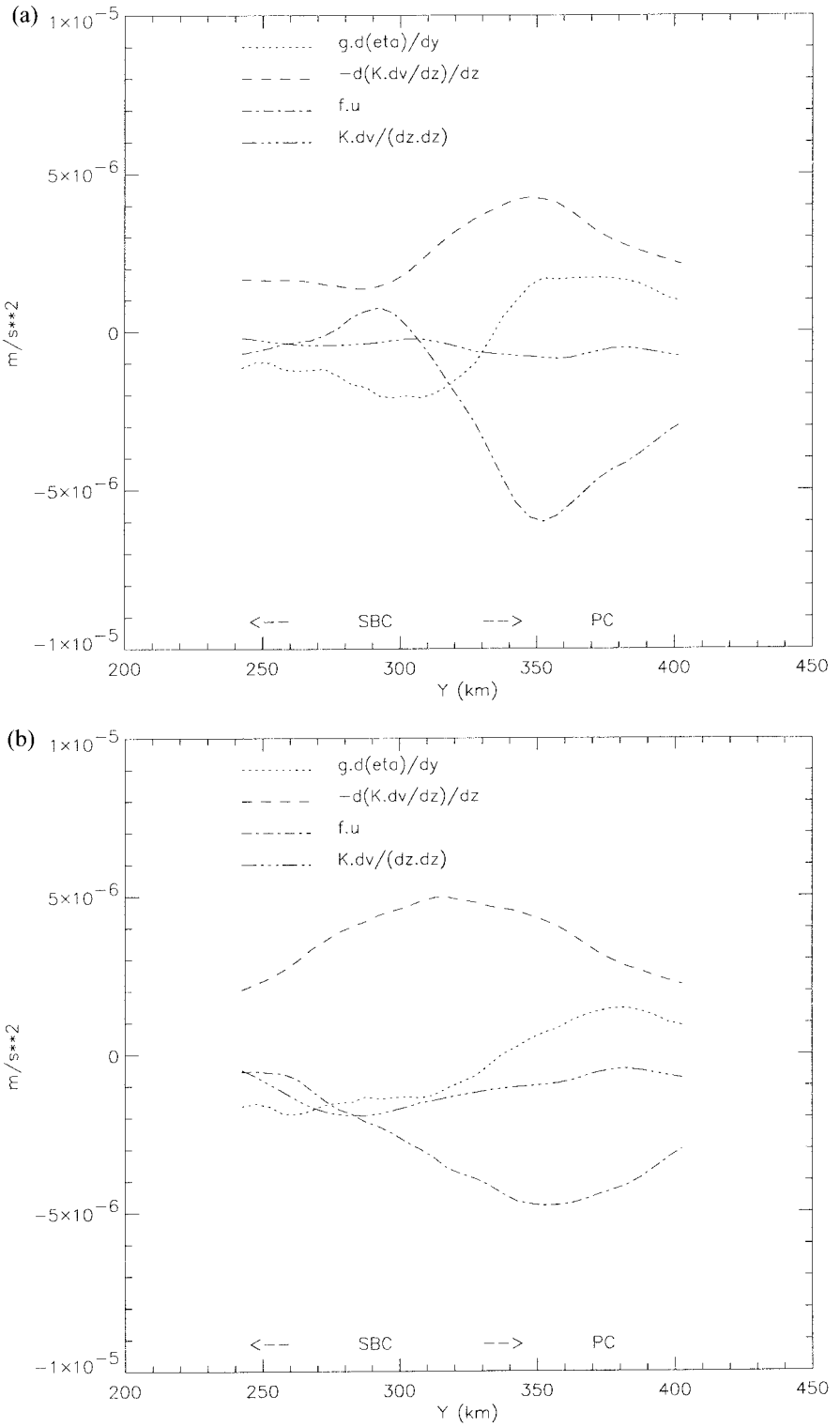

Figure 4. The three dominant terms: pressure gradient (dotted), vertical shear (dashed), and Coriolis (dash-dotted), and the term that represents friction at the base of the layer (dash with three dots), in the along-isobath momentum balance in the model's near-surface layer for (a) experiment A and (b) experiment B. Geographical locations along Y are SBC and PC.

the scenario exemplified by experiment B in which the equatorward wind is generally intense in the channel, balanced by the sum of an opposing poleward pressure gradient (Figure 4b) set up by the larger-scale weakening of the wind curl toward the south and poleward Coriolis force because of the cross-channel flow. In contrast, the equatorward wind is weaker in experiment A (Figure 4a), especially over the eastern half of the channel, so much so that the opposing poleward sea level slope, now further strengthened by a stronger along-channel gradient in wind curl, is able to force a poleward flow in the

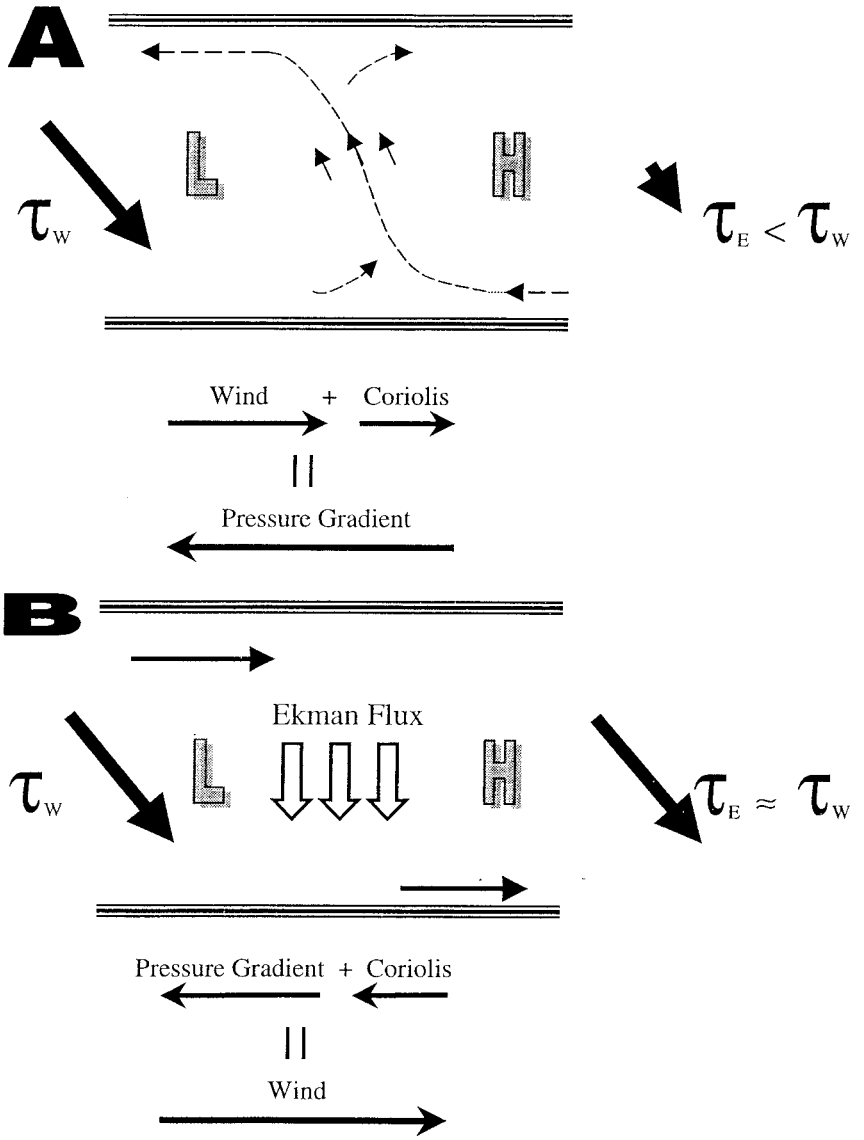

Figure 5. A schematic summary of flow balance in the Santa Barbara Channel for (a) experiment A, wind in east is weaker than that in west, and (b) experiment B, wind in east is of the same magnitude as that in west. Bold solid arrows on both sides of the channel denote winds, while other arrows inside the channel denote near-surface currents. Thin solid arrows below denote forces. The directions are poleward to left and equatorward to right.

channel, inducing in the process a northward cross-channel flow. (Contrast the region of positive "fu" curve in the channel in Figure 4a with the wholly negative fu curve of Figure 4b.) Equivalently, one can infer that in experiment A the excess pressure gradient caused by downward tilt of sea level toward the cyclone low in the western channel forces an onshore (northward) flux, which in turn reverses the wind-driven Ekman component at midchannel (280 km $< y <$ 310 km).

The balance in both cases are summarized schematically in Figure 5 and can be written as

Experiment A

Poleward Pressure = Equatorward

(Wind + Coriolis of South-to-North Cross Flow)

Experiment B

Equatorward Wind = Poleward

(Pressure + Coriolis of North-to-South Cross Flow).

Thus the near-surface flow in SBC can be viewed as being due to an imbalance between poleward (westward) pressure gradient and equatorward (eastward) wind stress. An excess of the former, caused by stronger along-channel gradient of the wind curl as a result of weakened wind in the eastern portion of the channel, generally leads to a northward cross-channel flow that tends to reinforce a cyclonic recirculation in the west, as well as to the likelihood that poleward flow develops in the channel (i.e., regime II discussed in section 1). The reverse (regime I) leads to a southward cross-channel Ekman flux near the surface, and the situation then is more akin to classical upwelling problems, which, in general, would result in equatorward flow in the channel. We have shown that the estab-

lishment of one regime versus the other depends crucially on the relative magnitude of the wind stresses west and east of the channel.

The momentum balance gives no clue as to how the western cyclone is formed, i.e., if the cyclone is a result of successions of regime II caused originally by equatorward weakening of the wind curl or is locally spun up (by wind curl or flow separation). It is clear that however it is produced, the cyclone dynamically contributes to the sea level tilt. Plate 2 and Figure 4 suggest that this dynamic influence is not restricted to the channel. North of Point Conception, the sea level slope term III changes sign to become positive. The change is more significant for experiment A, induced by the cyclone. The resulting equatorward acceleration reinforces that from the intense wind stress along the central California coast. Given that friction and other terms in the alongshore balance are small, these must be balanced by a poleward acceleration due to the Coriolis term. Thus the coastal jet acquires an offshore component that is most intense just south of PC, where both the wind and upward sloping of the sea level are maximum (Figure 4a), and the jet has a tendency to veer offshore (Plate 2 (left) in particular).

3.2. Balance in Other Experiments

To test the robustness of the above conclusions, a set of sensitivity experiments were conducted (Table 1). When CalCOFI T/S were not assimilated (experiment C or D), the strong poleward flow in early times of simulation, December 1997 and January 1998, for experiments A and B was now absent. However, because of upwelling in March and April, warmer water in experiments A and B was confined to the southern region (the SCB), and the dynamic balance in the channel was similar with or without CalCOFI T/S.

Finally, the model results also changed little when the values of x_s and y_s in the weighting function used to merge the NDBC with COADS winds were changed from 1.5° to 3° (experiment E). The results are also not sensitive to which of the two NDBC wind data in the southeasternmost stations (46045 in experiment A or 46025 in experiment F) was used for the wind station NDBC 46053.

4. Conclusions

Three dominant terms in the alongshore momentum balance of the near-surface currents in the Santa Barbara Channel are wind, which is equatorward, pressure gradient, which is poleward, and Coriolis due to cross-shore flows, which can be poleward or equatorward. In the SBC we have identified two distinct regimes of circulation that depend on the distribution of wind stress in the channel. For winds with approximately equal strengths west and east of the channel (or one with gradual change) the along-channel component produces southward Ekman flow across the channel that together with the pressure gradient, balances the wind. The along-channel flow then tends to be uniformly equatorward with no cyclonic recirculation in the west. This (regime I) would approximate the upwelling scenario described by *Harms and Winant* [1998]. On the other hand, for wind that is intense in the west but weak in the east, wind-induced Ekman flow is overcome by the south-to-north cross-channel flow generated by pressure gradient. This cross-channel flow occurs near and to the east of midchannel, where wind stress is weak. This (regime II) would tend to produce a cyclonic recirculation in the west and would correspond either to the cyclonic or relaxation characteristic patterns described by *Harms and Winant* [1998]. In both regimes the cross-channel flow serves as an important index that characterizes the imbalance between wind and pressure gradient.

A comparison of the pressure gradient terms in Figures 4a and 4b shows that they are of comparable magnitudes, although in the nonuniform wind case (Figure 4a), the presence of a cyclone in the west induced a larger sea level tilt. This suggests that a large portion of the sea level gradient is caused by larger-scale wind curl and heating over the SCB. One also ponders upon the chicken-and-egg question of whether the cyclone is formed by an aggregate of regime II events or is purely local, induced by localized wind curl and flow separation, say, and hence helps to promote the regime II event. This clearly requires further research.

Finally, the types of dynamic balance described here are of practical value. They help to identify forcing patterns that may then be used as key predictive parameters in hindcast and nowcast studies.

Acknowledgments. This work was funded by the Office of Naval Research (LYO) and the Mineral Management Service. Computing was performed at the Geophysical Fluid Dynamic Laboratory, Princeton, and the San Diego Supercomputer Center.

References

Allen, J. S., Models of wind-driven currents on the continental shelf, *Annu. Rev. Fluid Mech*., *12*, 389–433, 1980.

Auad, G., and M. C. Hendershott, The low-frequency transport in the Santa Barbara Channel: Description and forcing, *Cont. Shelf Res*., *17*, 779–802, 1997.

Chen, C.-S., and D.-P. Wang, Data assimilation model study of the Santa Barbara Channel circulation, *J. Geophys. Res*., *104*, 15,727–15,742, 1999.

Dorman, C. E., and C. D. Winant, The structure and variability of the marine atmosphere around the Santa Barbara Channel, *J. Geophys. Res*., *128*, 261–282, 2000.

Harms, S., and C. D. Winant, Characteristic patterns of the circulation in the Santa Barbara Channel, *J. Geophys. Res*., *103*, 3041–3065, 1998.

Hayward, T. L., et al., The state of the California Current in 1998–99: Transition to cool-water conditions, *CalCOFI Rep*., *40*, 29–62, 1999.

Hickey, B. M., Circulation over the Santa Monica-San Pedro basin and shelf, *Prog. Oceanogr*., *30*, 37–115, 1992.

Large, W. G., and S. Pond, Open ocean momentum flux measurements in moderate to strong winds, *J. Phys. Oceanogr*., *11*, 324–336, 1981.

Oey, L.-Y., Flow around a coastal bend: A model of the Santa Barbara Channel eddy, *J. Geophys. Res*., *101*, 16,667–16,682, 1996.

Oey, L.-Y., A forcing mechanism for the poleward flow off the southern California coast, *J. Geophys. Res*., *104*, 13,529–13,539, 1999.

Oey, L.-Y., and P. Chen, A nested-grid model simulation of the Norwegian coastal current, *J. Geophys. Res*., *97*, 20,063–20,086, 1992.

Winant, C. D., and C. E. Dorman, Seasonal patterns of surface wind stress and heat flux over the Southern California Bight, *J. Geophys. Res*., *102*, 5641–5653, 1997.

T. Hayward, Marine Life Research Group, Scripps Institute of Oceanography, La Jolla, CA 92093.

M. Hendershott and C. Winant, Center for Coastal Studies, Scripps Institute of Oceanography, La Jolla, CA 92093.

L.-Y. Oey, Atmospheric and Oceanic Science Program, Princeton University, Princeton, NJ 08544. (lyo@princeton.edu)

D.-P. Wang, Marine Science and Research Center, State University of New York at Stony Brook, Stony Brook, NY 11794.

(Received November 8, 1999; revised December 26, 2000; accepted January 12, 2001.)